Mon. Not. R. Astron. Soc. **392,** 1388–1396 (2009) doi:10.1111/j.1365-2966.2008.14028.x

Measurement of the baryonic acoustic oscillation scale in 21 cm intensity fluctuations during the reionization era

Kirsty J. Rhook,[1★] Paul M. Geil[2★] and J. Stuart B. Wyithe[2★]

[1] *Institute of Astronomy, Madingley Road, Cambridge CB3 0HA*
[2] *School of Physics, University of Melbourne, Parkville, Victoria, Australia*

Accepted 2008 September 30. Received 2008 September 3; in original form 2008 March 19

ABSTRACT

It has recently been suggested that the power spectrum of redshifted 21 cm fluctuations could be used to measure the scale of baryonic acoustic oscillations (BAOs) during the reionization era. The resulting measurements are potentially as precise as those offered by the next generation of galaxy redshift surveys at lower redshift. However, unlike galaxy redshift surveys, which in the linear regime are subject to a scale-independent galaxy bias, the growth of ionized regions during reionization is thought to introduce a strongly scale-dependent relationship between the 21 cm and mass power spectra. We use a seminumerical model for reionization to assess the impact of ionized regions on the precision and accuracy with which the BAO scale could be measured using redshifted 21 cm observations. For a model in which reionization is completed at $z \sim 6$, we find that the constraints on the BAO scale are not systematically biased at $z \gtrsim 6.5$. In this scenario, and assuming the sensitivity attainable with a low-frequency array comprising 10 times the collecting area of the Murchison Widefield Array, the BAO scale could be measured to within 1.5 per cent in the range $6.5 \lesssim z \lesssim 7.5$.

Key words: diffuse radiation – large-scale structure of Universe.

1 INTRODUCTION

The imprint of baryonic acoustic oscillations (BAOs) on the mass power spectrum (PS) provides a cosmic yardstick that can be used to measure the dependence of both the angular diameter distance and Hubble parameter on redshift. The wavelength of a BAO is related to the size of the sound horizon at recombination. Its value depends on the Hubble constant and on the dark matter and baryon densities. However, it does not depend on the amount or nature of dark energy. Thus, measurements of the angular diameter distance and Hubble parameter can in turn be used to constrain the possible evolution of dark energy with cosmic time (e.g. Eisenstein, Hu & Tegmark 1998; Eisenstein 2002).

Galaxy surveys have proved to be a powerful probe of the linear PS on large scales, and therefore provide a means to measure the BAO scale (e.g. Blake & Glazebrook 2003; Hu & Haiman 2003; Seo & Eisenstein 2003, 2005; Glazebrook & Blake 2005; Seo & Eisenstein 2007; Angulo et al. 2008). Indeed, the analyses of the galaxy PS from the Sloan Digital Sky Survey and 2d Field Galaxy Redshift Survey have uncovered a BAO signal (e.g. Cole et al. 2005; Eisenstein et al. 2005; Percival et al. 2007; Okumura et al. 2008; Gaztanaga, Cabre & Hui 2008a; Gaztanaga, Miquel & Sanchez 2008b), providing incentive for deeper all-sky galaxy surveys, using telescopes like the SKA,[1] Pan-STARRS[2] and the LSST,[3] to measure the BAO scale and hence the dark energy equation of state more accurately.

Galaxy redshift surveys are best suited for studies of the dark energy equation of state at relatively late times ($z \lesssim 3$) due to the difficulty of obtaining accurate redshifts for a sufficiently large number of high-redshift galaxies. Although the detection of the Integrated Sachs–Wolfe effect puts some constraints on the integrated role of dark energy above $z \sim 1.5$ [see e.g. Giannantonio et al. (2008) and references therein], we currently have very limited information about the nature of dark energy at a high redshift. If dark energy behaves like a cosmological constant, then its effect on the Hubble expansion is only significant at $z \lesssim 1$ and becomes negligible at $z \gtrsim 2$. In this case, studies of the BAO scale at a low redshift would provide the most powerful constraints. However, as the origin of dark energy is not understood we cannot presume a priori which redshift range should be studied in order to provide optimal constraints on proposed models. Probes of dark energy at higher redshifts have been suggested. These include the measurements of the PS from a Lyα forest survey which could potentially be used to probe the evolution of dark energy through the measurement of the BAO scale for redshifts as high as $z \sim 4$ (McDonald & Eisenstein 2007). Similarly,

★E-mail: krhook@ast.cam.ac.uk (KJR); pgeil@physics.unimelb.edu.au (PMG); swyithe@unimelb.edu.au (JSBW)

[1] Square Kilometre Array: http://www.skatelescope.org
[2] Panoramic Survey Telescope and Rapid Response System: http://pan-starrs.ifa.hawaii.edu/public
[3] Large Synoptic Sky Survey: http://www.lsst.org

studying the temporal variation of high-resolution quasar spectra may probe the evolution of dark energy through the Sandage–Loeb test in the window $2 < z < 5$ (Corasaniti, Huterer & Melchiorri 2007). Measurements of the BAO scale in the reionization era ($z > 6$) are likely to be complementary to the constraints at lower redshifts provided by these techniques.

It has recently been suggested that observations of 21 cm intensity fluctuations might provide an additional avenue to measure the mass PS (e.g. Bowman, Morales & Hewitt 2006; McQuinn et al. 2006; Mao et al. 2008) and that future low-frequency arrays could be used to measure the BAO scale at a range of redshifts (Chang et al. 2008; Mao & Wu 2008; Wyithe, Loeb & Geil 2008). Redshifted 21 cm surveys are sensitive to neutral hydrogen regardless of whether it is part of a resolved object. As a result, at high redshifts such surveys may be more efficient in measuring the large-scale mass distribution than galaxy redshift surveys, which must identify a very large number of individual galaxies. Furthermore, spectroscopic emission line surveys have the advantage of probing a precisely defined redshift interval, which is unlikely to be true of a traditional galaxy survey (see Simpson & Bridle 2006).

Planned low-frequency arrays such as the Murchison Widefield Array[4] (MWA) and Low Frequency Array[5] are designed to measure the PS of 21 cm fluctuations at $z > 6$ in order to probe the reionization era. Wyithe et al. (2008) have argued that while the first generation of low-frequency arrays will not have sufficient sensitivity to precisely determine the BAO scale, future extensions could have the sensitivity to detect the BAO scale with promisingly small errors. Wyithe et al. (2008) assumed a semi-analytic model which predicts a scale-independent value for the effective bias between the linear matter PS and the 21 cm PS. However, the 21 cm bias is expected to be strongly scale-dependent, especially towards the end of reionization when many ionized bubbles percolate through the intergalactic medium (IGM), creating an excess of power on scales larger than the characteristic bubble size (e.g. Furlanetto, Zaldarriaga & Hernquist 2004). In this paper, we explore whether the scale dependence of the 21 cm bias will compromise the ability of redshifted 21 cm observations to measure the BAO scale (Mao & Wu 2008). We begin by reviewing the expected BAO signal and 21 cm PS in Section 2. We describe the observation of the 21 cm PS, including a discussion of the noise considerations in Section 3. In Section 4, we describe our fitting procedure for recovering the BAO scale, and present our error analysis before concluding in Section 5. To calculate these errors we adopt a set of cosmological parameters similar to those derived from the 3-year *Wilkinson Microwave Anisotropy Probe (WMAP)* data (Spergel et al. 2007), namely $\Omega_m = 0.24, \Omega_\Lambda = 0.76, h = 0.73, \sigma_8 = 0.76$ and $\Omega_b = 0.042$.

2 THEORETICAL BACKGROUND

The sound speed at recombination (s) determines the length scale of the acoustic peaks in both the cosmic microwave background (CMB) anisotropies and the linear matter PS. We refer to this length as the BAO scale. The comoving horizon size at decoupling (r) may be determined from the knowledge of Ω_m and Ω_b, and an understanding of the physics governing a baryon–photon fluid (Page et al. 2003). Komatsu et al. (2008) calculate this length scale to be 146 ± 1.8 Mpc for the cosmological parameters extracted from the 5-year *WMAP* data. The corresponding angular scale $\theta_A = r/D_A(z_{\rm rec})$ is closely related to the position of the first acoustic peak in the CMB PS, which occurs at the scale of the mode which has compressed once at the time of decoupling (see Page et al. 2003). Following decoupling, the same acoustic scale is imprinted in the matter PS, albeit with a different phase. This signature is expected to be preserved on large scales where non-linear gravitational effects are small. Therefore, the BAO scale may be used as a standard ruler to test the geometry of the Universe and the role of dark energy.

2.1 Theoretical expectations for the redshifted 21 cm power spectrum

Neutral hydrogen radiates at 21 cm due to the hyperfine transition between the singlet and triplet ground states. Assuming a contrast between the kinetic temperature of the IGM T_k and the CMB temperature $T_{\rm CMB}$, and efficient coupling of the spin temperature T_s to T_k, the 21 cm signal will mirror the underlying density of neutral hydrogen. The Lyα and X-ray flux emitted by the first galaxies are expected to ensure these conditions hold during most of the reionization era (see e.g. Furlanetto 2006). A radio interferometer is sensitive to fluctuations in the brightness temperature of neutral gas. For gas of mean cosmic density, the expected temperature brightness contrast in redshifted 21 cm emission is

$$\begin{aligned}\delta T_b &= \frac{T_b - T_{\rm CMB}}{(1+z)}(1-e^{-\tau}) \\ &\approx 22\ {\rm mK}\ x_{\rm H\,I}\left(1-\frac{T_{\rm CMB}}{T_s}\right)\left(\frac{\Omega_b h^2}{0.02}\right) \\ &\quad\times\left[\left(\frac{1+z}{7.5}\right)\left(\frac{0.24}{\Omega_m}\right)\right]^{1/2} \\ &\equiv \delta\bar{T}_b \bar{x}_{\rm H\,I}\end{aligned} \tag{1}$$

where τ is the optical depth of the neutral gas to 21 cm radiation and $\bar{x}_{\rm H\,I}$ is the mass-weighted neutral fraction of hydrogen in the IGM.

Allowing for fractional fluctuations in the baryonic matter density $\delta(\boldsymbol{x})$, ionized fraction $\delta_x(\boldsymbol{x})$ and peculiar gas velocity $\delta_v(\boldsymbol{x}) = \frac{1+z}{H(z)}\frac{dv_r}{dr}(\boldsymbol{x})$ (where $\frac{dv_r}{dr}$ is the peculiar velocity of the gas),[6] the spatial dependence of the brightness temperature fluctuations may be written as (e.g. Mao & Wu 2008)

$$\begin{aligned}\delta T_b(\boldsymbol{x}) &= \delta\bar{T}_b[1-(1-\bar{x}_{\rm H\,I})(1+\delta_x)](1+\delta)(1-\delta_v) \\ &\quad\left(1-\frac{T_{\rm CMB}}{T_s}\right).\end{aligned} \tag{2}$$

Assuming the peculiar velocity effect is described by the linear theory result from Kaiser (1987), i.e. $\delta_v(\boldsymbol{k}) = -f\mu^2\delta(\boldsymbol{k})$ (note that $f \rightarrow 1$ in the high-redshift limit), where $\mu = \boldsymbol{k}\cdot\boldsymbol{n}$ denotes the angle between the line of sight and the Fourier vector $\boldsymbol{k}$, the angle-dependent 21 cm PS may be written as (e.g. Mao & Wu 2008)

$$\begin{aligned}P_{21}(\boldsymbol{k}, z) = \delta\bar{T}_b^2\,\{&[\bar{x}_{\rm H\,I}^2 P_{\delta\delta} - 2\bar{x}_{\rm H\,I}(1-\bar{x}_{\rm H\,I})P_{\delta x} \\ &+ (1-\bar{x}_{\rm H\,I})^2 P_{xx}] + 2f\mu^2[\bar{x}_{\rm H\,I}^2 P_{\delta\delta} - \bar{x}_{\rm H\,I}(1-\bar{x}_{\rm H\,I})P_{\delta x}] \\ &+ f^2\mu^4\bar{x}_{\rm H\,I}^2 P_{\delta\delta}\}\,.\end{aligned} \tag{3}$$

The values of $P_{\delta\delta}, P_{xx}$ and $P_{\delta x}$ denote the linear matter power spectrum, ionization power spectrum and ionization–density cross power spectrum, respectively. In general, the 21 cm PS will display complex angle and redshift-dependent structure. The difference in the angular dependence modulating the cosmological ($P_{\delta\delta}$)

[4] http://www.haystack.mit.edu/ast/arrays/mwa

[5] http://www.lofar.org

[6] Variations in the local Ly-α flux may also result in fluctuations in the signal through T_s (e.g. Barkana & Loeb 2005b).

and astrophysical ($P_{\delta x}$, P_{xx}) components may be able to be exploited to constrain both cosmological and astrophysical parameters (e.g. Barkana & Loeb 2005a; Mao & Wu 2008). The spherically averaged 21 cm PS may be more simply related to the underlying mass PS via

$$P_{21}(k, z) = b_{21}(k, z)^2 P_l(k, z) D^2(z), \tag{4}$$

where P_l is the primordial linear matter PS extrapolated to $z = 0$ calculated using CMBFAST (Seljak & Zaldarriaga 1996) and $D(z)$ is the linear growth factor between redshift z and the present. In equation (4), the pre-factor $b_{21}(k, z)$ is a term which is analogous to galaxy bias (but which has units of mK). However, in contrast to galaxy redshift surveys, the value of b_{21} can be scale-dependent, even in the linear regime, as a result of the long-range, non-gravitational correlations introduced into the ionization structure of the IGM by the formation of H II regions. Whilst peculiar velocity effects will be present, Seo & Eisenstein (2005) find that the BAO signal is preserved in the matter PS at $z \sim 3$. Furthermore, Seo et al. (2008) and Shaw & Lewis (2008) show that even the effect of non-linear redshift space distortions on the spherically averaged matter PS may be able to be corrected to high accuracy.

Equation (4) implicitly assumes that the gravitational dynamics governing the large-scale structures probed are well described by linearized fluid equations. Non-linear gravitational dynamics will be increasingly important at low redshift. However, at the redshifts of interest here ($z > 6$) non-linear evolution is unlikely to play a significant role (see e.g. Crocce & Scoccimarro 2008; Mao & Wu 2008). Mao et al. (2008) find that the cut-off in the maximum wavenumber probed by redshifted 21 cm PS in the range $7 < z < 9$ has little effect on the constraints on cosmological parameters.

2.2 Model for the evolution of the 21 cm signal

In the early stages of reionization when most of the hydrogen is still neutral, the bias between the linear matter PS and the 21 cm PS, b_{21}, is well approximated by a constant with units of temperature. However, the bias is expected to depend on scale during the process of reionization since galaxies preferentially form in overdense regions, resulting in early formation of ionized bubbles from an overdense IGM. This effect can be modelled semi-analytically (e.g. Wyithe & Morales 2007), or with full numerical calculations of reionization (e.g. McQuinn et al. 2007a,b; Trac & Cen 2007). Recently, semi-numerical schemes have been devised which allow efficient calculation of the large-scale ionization field (Mesinger & Furlanetto 2007; Zahn et al. 2007; Geil & Wyithe 2008). We use simulations computed using the method described in Geil & Wyithe (2008) to model b_{21}. We refer the reader to the discussion of the semi-numerical modelling in that paper and to the discussion of the underlying semi-analytic model for the reionization of the IGM in Wyithe & Morales (2007). Only a brief overview of the assumptions and characteristics of the model(s) is included here.

Wyithe & Morales (2007) describe a semi-analytic model for the density- and scale-dependent ionization fraction of the IGM. This model assumes that a certain fraction of the mass in collapsed haloes forms galaxies, and that these galaxies produce ionizing photons with some efficiency. The ionization due to galaxies is opposed by the density-dependent recombination rate. An overdensity-dependent rate of ionization may then be calculated as a function of scale. For the examples shown in this paper, the model parameters are tuned such that reionization is completed by $z = 6$. Wyithe & Morales (2007) use this model to explore the 21 cm brightness temperature contrast as a function of scale and redshift. Geil & Wyithe (2008) use these scale- and overdensity-dependent predictions for the ionized gas fraction of the IGM to generate realizations of the real-space density and ionization fraction of a region of the IGM. In this paper, we use the seminumerical model to compute the 21 cm bias b_{21}. We note that our calculation does not include redshift space distortions (Barkana & Loeb 2005a) which are not captured by the model used in this paper. The free parameters include the star formation efficiency, escape fraction of ionizing photons and the minimum halo virial temperature for star formation in neutral and ionized regions of IGM (for which we take 10^4 and 10^5 K, respectively). The seminumerical simulation was performed in a cube with 256^3 resolution elements and of side length 3 Gpc (comoving).

In Fig. 1, we show the model 21 cm PS at $z = 6.5$, 7, 7.5 and 8, corresponding to average volume-weighted neutral fractions $x_{\mathrm{H\,I}} =$ 0.14, 0.28, 0.42, 0.53. The left-hand panels show the ionized gas distribution from the semi-numerical simulations for a box with side length 3 Gpc (comoving). The panels in the second column show the spherically averaged model 21 cm PS (grey lines). The panels in the third column show the model 21 cm bias (grey lines). The far right-hand panels show the BAO component of the PS, defined as the difference between the 21 cm PS and a reference 21 cm PS computed from a mass PS without baryons, $P_{\mathrm{l,nb}}(k)$. The model BAO component, $b_{21}^2(k)\, D^2(z)\, [P_l(k) - P_{\mathrm{l,nb}}(k)]$, is shown in grey. The model PS is reproduced in Fig. 2.

2.3 Fitting formula for 21 cm power spectra

Following Seo & Eisenstein (2005), we parametrize the fit to the semi-numerical model of the spherically averaged 21 cm PS as

$$P_{21,\mathrm{fit}}(k, z) = B^2(k)\, D^2(z)\, P_l(k/\alpha) + AP(k), \tag{5}$$

where $AP(k) = c_0 + c_1 k + c_2 k^2$ is a term to describe anomalous power and $B(k) = b_0 + b_1 k + b_2 k^2 + b_3 k^3$ is the fitted bias in units of mK. The 'dilation' or 'phase' parameter α allows for a dilation/contraction of the matter PS used to fit the 21 cm PS. In our case, the input value of α is unity since we are assuming that we know the cosmological parameters governing P_l. Seo & Eisenstein (2005) note that for the parametrization of the PS in equation (5), the errors in the known values of the wavenumber dilation parameter α directly translate into the errors in the measured BAO scales. In Section 4.2, we calculate the expected redshift-dependent errors $\Delta\alpha$ for an observational campaign which is described in Section 3.

The anomalous power term allows for the distortion of the matter PS due to non-linear mode coupling. Seo & Eisenstein (2005) find that by subtracting a smooth function (AP) from the matter PS derived from their N-body simulations, they are able to recover the shape of the matter PS and thus the BAO signal. Our semi-numerical model is intrinsically linear, and so does not include anomalous power. However, we explore the possible effect of anomalous power on the measurement of the BAO scale by including the correction term AP in the fitted PS. Inclusion of this term approximates the effect of degeneracy between anomalous power and scale-dependent bias. In this paper, we present results using fits both with and without the AP term. Note that the degeneracy between the parameters governing the anomalous power and bias terms means that the polynomial fits to these functions cannot be interpreted physically when the AP term is included (see Section 4). However, we find that this degeneracy does not significantly hinder the determination of α.

More detailed cosmological constraints may be obtainable if the line of sight and transverse BAO scales could be measured independently (see Wyithe et al. 2008 and references therein, and also

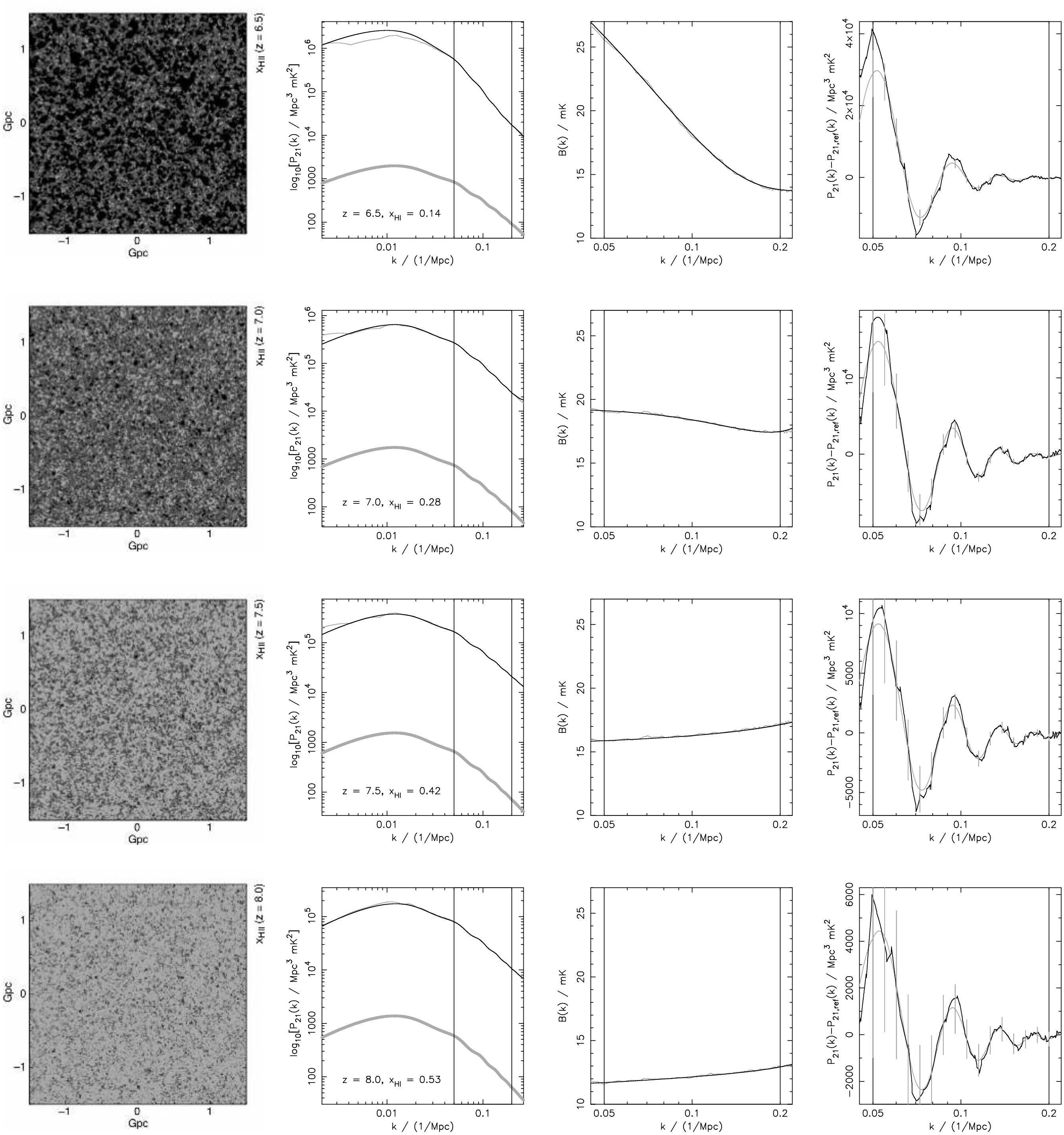

Figure 1. Model power spectra and fits assuming a third-order polynomial bias and no anomalous power. The left-hand panels show the ionization maps corresponding to the redshifts of $z = 6.5$, 7.0, 7.5 and 8.0. The panels in the second column display the corresponding model (*grey*) and fitted (*black*) 21 cm PS, and the linear matter PS (*thick grey* line). The panels in the third column show the fitted (*black*) and model (*grey*) scale-dependent bias. In the far right-hand panels, we plot the difference between the model 21 cm PS with and without baryons (*grey*), and the recovered 21 cm PS with and without baryons (*black*), as described in the text. The *grey* error bars correspond to spherically averaged noise as described in Section 3. In each panel, the vertical lines indicate the range of k values used for the fit.

Okumura et al. 2008; Gaztanaga et al. 2008a,b for recent constraints from galaxy surveys). Indeed, a low-frequency array is naturally suited to measuring both the line of sight and transverse components of the 21 cm PS (see Section 3). Such an analysis would require modelling of the peculiar velocity effects which give rise to the angular dependence of the 21 cm PS in equation (3). As mentioned, the model adopted for the 21 cm PS does not include peculiar velocities. However, we note that the above fitting formula could be readily generalized to characterize the ionization and cross density-ionization power spectra needed to describe the angular dependence

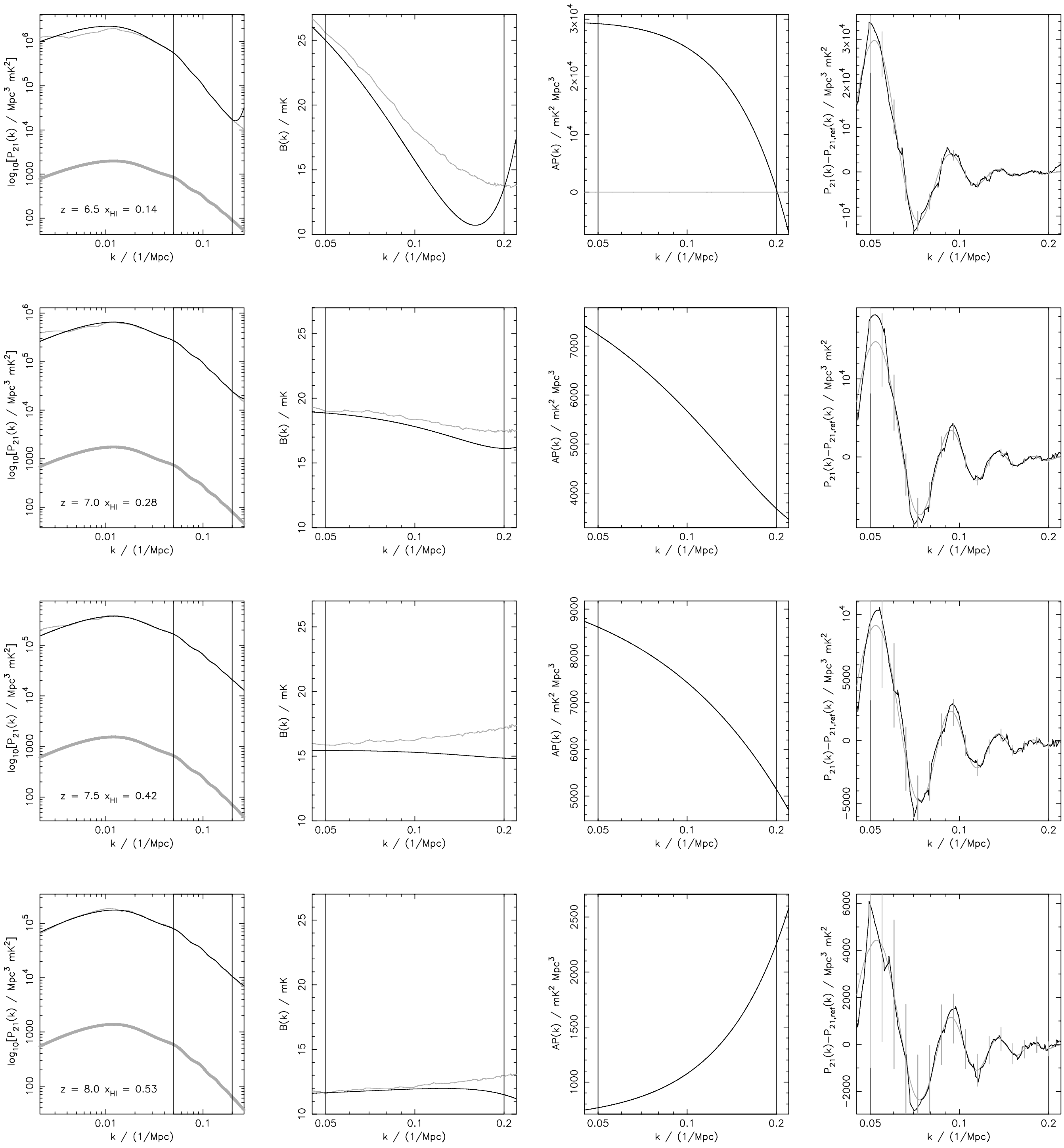

Figure 2. Model power spectra and fits assuming a third-order polynomial bias and quadratic anomalous power for the same simulation data as Fig. 1. The first column of panels display the model (*grey*) and fitted (*black*) 21 cm PS, and the linear matter PS (*thick grey* line) at redshifts of $z = 6.5$, 7.0, 7.5 and 8.0. The panels in the second column show the fitted (*black*) and model (*grey*) scale-dependent bias. The anomalous power component of the fit is plotted in the third column. In the far right-hand panels we plot the difference between the model PS with and without baryons (*grey*), and the recovered PS with and without baryons (*black*), as described in the text. The *grey* error bars correspond to spherically averaged noise as described in Section 3. In each panel, the vertical lines indicate the range of k values used for the fit.

in equation (3). This would allow constraints on the dilation parameter, and therefore the BAO scale, both perpendicular and parallel to the line of sight to be extracted from the 21 cm PS. The signal-to-noise ratio estimates in Wyithe et al. (2008) suggest that the MWA5000 will be similarly sensitive to each of these scales.

3 MEASUREMENT OF 21 cm POWER SPECTRA

In this section, we discuss the sensitivity of a low-frequency array to the 21 cm PS. The sensitivity to the PS depends on the array design (e.g. total collecting area and antenna distribution) as well as the observation strategy (e.g. total integration time). We consider a low-frequency array which would be a 10-fold extension of the MWA. We refer to this array as the MWA5000 (McQuinn et al. 2006). The MWA5000 would consist of 5000 antennas (with each antenna composed of a tile of 4 × 4 cross dipoles) with effective collecting area $A_e \sim 16\lambda^2/4\,\mathrm{m}^2$, where $\lambda = 0.21(1+z)\,\mathrm{m}$ is the observed wavelength. The dipoles will be sensitive to a wide range of frequencies which translate into redshifts spanning the expected extent of reionization. However, we assume that the receiver will limit the bandpass to a selected $B_{\rm tot} = 32$ MHz window per observation. We assume that the antennas are distributed with constant density in a core of radius 80 m (within which the $u - v$ coverage is very high), with the remainder distributed with a radially symmetric density profile $\rho \propto r^{-2}$ out to a radius of 1 km (so that the maximum baseline is ∼2 km).

We use the prescription from Bowman et al. (2006) for the three-dimensional (3d) sensitivity of an array to the 21 cm PS. The array sensitivity is expressed in terms of the wavevector components which are orthogonal $k_\perp$ and parallel $k_\parallel$ to the line of sight. The modulus of the wavenumber is then given by $k = |\boldsymbol{k}| = \sqrt{k_\parallel^2 + k_\perp^2}$. The sensitivity at large k depends crucially on the angular resolution of the array (and therefore the maximum baseline), the bandpass over which the measurement is made $\Delta\nu$, the integration time $t_{\rm int}$ and the density of baselines which measures a particular k mode. The noise may be divided into two distinct components. The thermal noise component ΔP_{21}, N is proportional to the sky temperature, where $T_{\rm sky} \sim 250(\frac{1+z}{7})^{2.6}$ K at the frequencies of interest, and may be written as

$$\Delta P_{21,\rm N}(\boldsymbol{k}) = \left[\frac{T_{\rm sky}^2}{\Delta\nu t_{\rm int}}\frac{D^2\Delta D}{n(k_\perp)}\left(\frac{\lambda^2}{A_{\rm e}}\right)^2\right]\frac{1}{\sqrt{N_c}}, \quad (6)$$

where D is the comoving distance to the centre of the survey volume which has a comoving depth ΔD. Here, $n(k_\perp)$ is the density of baselines which observe a wavevector with transverse component $k_\perp$. In the denominator, N_c denotes the number of modes observed in a k-space volume d^3k. In terms of the k-vector components, $N_c = 2\pi k_\perp \Delta k_\perp \Delta k_\parallel \mathcal{V}/(2\pi)^3$, where $\mathcal{V} = D\Delta D(\lambda^2/A_{\rm e})$ is the observed volume. Note that this calculation of N_c incorporates the fact that k modes which do not fit in the bandpass $\Delta\nu$ are not observable. The sample variance component of the noise is given by $\Delta P_{21,SV}(\boldsymbol{k}) = P_{21}(\boldsymbol{k})/\sqrt{N_c}$. The sensitivity will improve with the square root of the number of independent fields observed. The total noise may therefore be expressed by

$$\Delta P_{21}(k_\perp, k_\parallel, z) = \frac{\Delta P_{21,N}(k_\perp, k_\parallel, z) + \Delta P_{21,SV}(k_\perp, k_\parallel, z)}{\sqrt{N_{\rm fields} B_{\rm tot}/\Delta\nu}}. \quad (7)$$

For the purposes of constraining the parameters in equation (5), we average equation (7) over the viewing angle to obtain the spherically averaged noise $\Delta P_{21}(k, z)$. Note that this calculation assumes perfect foreground removal over a bandpass with width $\Delta\nu$ [see McQuinn et al. (2006) for a discussion of the relationship between foreground removal and bandpass width]. In Section 4, we explore the effect of the choice of $\Delta\nu$ on the errors in the measurement of α.

We assume that the spherically averaged PS is measured in $n_k = 32$ logarithmically spaced intervals with end points in the range $0.05 \le k \le 0.2\,\mathrm{Mpc}^{-1}$. Wavenumbers below this range would not fit within the nominal bandwidth of ∼8 MHz at the redshifts of interest. Above $0.2\,\mathrm{Mpc}^{-1}$, the BAO signal becomes very weak and the matter PS may be non-linear. The binning in k space, which is approximately equivalent to the bin widths of $\Delta k \sim k/20$, is motivated by the scale of the expected BAO features. For clarity, the grey error bars in Figs 1 and 2 represent the uncertainty on the spherically averaged PS for larger spectral bins with width $\Delta k = k/10$. We assume that three fields are observed ($N_{\rm fields} = 3$) for 1000 h each. Given the field of view at these redshifts, this would correspond to surveying a few per cent of the sky.

4 FITS TO 21 cm POWER SPECTRA

In this section, we describe the results of fits to the modelled 21 cm PS using the parametrized form in equation (5).

4.1 χ^2 minimization

We adopt the χ^2 function as an indicator for the 'goodness of fit' of our model,

$$\chi^2(\boldsymbol{p}) = \sum_{i=1}^{n_k}\left[\frac{P_{21}(k,z) - P_{21,\rm fit}(\boldsymbol{p},k,z)}{\sigma_i}\right]^2, \quad (8)$$

where $\sigma_i = \Delta P_{21}(k, z)$ and $\boldsymbol{p} \equiv \{p_j\} = (\alpha, b_0, b_1, b_2, b_3, c_0, c_1, c_2)$ is a vector containing the model parameters. The index i refers to the n_k discrete values of k corresponding to each data bin (see Section 3). We restrict our fitting to the range $0.05 \le k \le 0.2\,\mathrm{Mpc}^{-1}$.

We have adapted the Numerical Recipes routines (Press et al. 1992) which implement the Levenberg–Marquardt technique to iteratively find the parameter set which minimizes the χ^2 function for a model which is non-linear in its parameters $\boldsymbol{p}$. In Figs 1 and 2, we show the resulting fits for the cases with a third-order polynomial bias (black lines), with and without a quadratic anomalous power term, respectively. The panels in the second column of Fig. 1 (and the first column in Fig. 2) show the fitted spherically averaged 21 cm PS as well as the linear matter PS. The panels in the third column of Fig. 1 (and second column of Fig. 2) show the fitted 21 cm bias. In Fig. 2, the panels in the third column show the fitted *AP* term (note that the input term is zero since non-linear effects are not incorporated into the seminumeric code we have used to generate the ionization maps.). The far right-hand panels in each of Figs 1 and 2 show the BAO component of the fitted PS, $B^2(k)\, D^2(z)\, P_{\rm l}(k) + AP(k) - b_{21}^2(k)\, D^2(z)\, P_{\rm l,nb}(k)$. The noise in the fitted BAO component is due to the noise in the model calculation of the bias b_{21}.

The fit to the 21 cm PS is very good in all cases. When the anomalous power term is included there is a trade-off between the power in the 21 cm PS associated with the bias B and that due to *AP*, indicating some degeneracy. However, as we show in the next section, this degeneracy does not significantly bias the constraints on the BAO scale. It may of course be possible to alleviate the degeneracies between the bias and the *AP* parameters by putting some physically/numerically motivated priors on the values of c_0, c_1 and c_2.

4.2 Uncertainty in the measured BAO scale

After marginalizing over the remaining fit parameters, we may interpret the error in α for our fits as the fractional uncertainty in the measurement of the BAO scale (Seo & Eisenstein 2005). The Fisher matrix $\mathbf{F}$ is given by (Tegmark, Taylor & Heavens 1997)

$$F_{ij} = \sum_{k=0}^{n_p}\sum_{l=0}^{n_p}\frac{\partial P_{21,\rm fit}}{\partial p_i}\frac{\partial P_{21,\rm fit}}{\partial p_j}, \quad (9)$$

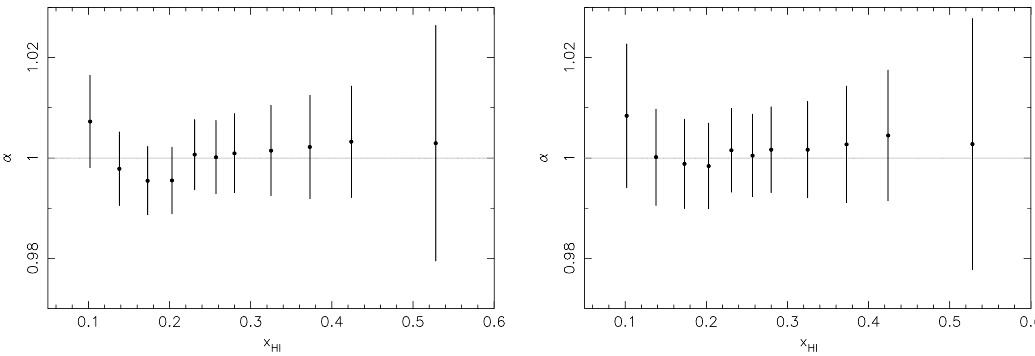

Figure 3. Fitted values and uncertainty for the α using a fit with third-order polynomial bias with (left-hand panel) and without (right-hand panel) a quadratic anomalous power term. The error bars represent the 1σ (68.3 per cent) confidence intervals calculated using from the Fisher matrix by marginalizing over all of the other parameters in the fit.

where n_p is the dimension of $\boldsymbol{p}$ and all derivatives are evaluated using the best-fitting $\boldsymbol{p}$. Since we expect the noise in 21 cm PS to be Gaussian, we may invoke the Cramer–Rao theorem to estimate the 1σ(68.3 per cent) confidence interval around the best-fitting value of α from $\mathbf{F}$. Assuming that all other parameters are marginalized over this implies errors around the best-fitting values for α of

$$\Delta\alpha = \left(F_{11}^{-1}\right)^{-1/2}. \tag{10}$$

In Fig. 3, we plot the best-fitting values of α and the associated 1σ error as calculated in equation (10) for several redshifts in the range $6.4 \le z \le 8$ corresponding to average neutral fractions of $0.1 \lesssim x_{\rm H\,I} \lesssim 0.5$ for our reionization model. The left-hand panel of Fig. 3 assumes a fitted 21 cm PS with no anomalous power term, whereas the fitted PS used to generate the plot in the right-hand panel includes the *AP* term. In each panel, the grey horizontal line indicates the input value $\alpha = 1$. Note that the recovered values of α deviate from the input values at $x_{\rm H\,I} \sim 0.1$–0.2 ($z \sim 6.4-6.7$). However, for the observing strategy and k-space binning chosen, this deviation is within the estimated 1σ statistical error (although only just at $z \sim 6.4$ where the neutral fraction is ∼10 per cent). As reionization nears completion ($x_{\rm H\,I} \rightarrow 0.1$), the 21 cm bias becomes most strongly scale-dependent in the range $0.05 \lesssim k \lesssim 0.2\,{\rm Mpc}^{-1}$. The increasing systematic error towards $z \sim 6.4$ is therefore a result of the (relatively) low noise level in the 21 cm PS at these redshifts combined with the increasingly strong evolution of the bias function within the fitted range of k values.

We find that the statistical errors are slightly larger when we include the extra parameters required to describe the anomalous power (since the matrix $\mathbf{F}$ is not diagonal). We note that our estimate of the attainable errors on the phase/dilation parameter α are a minimum in the sense that (i) we have assumed perfect foreground removal across each bandpass with width 8 MHz for a total bandwidth of 32 MHz and (ii) we have invoked the Cramer–Rao theorem regarding the minimum 1σ error on a parameter from the Fisher matrix of the best-fitting model.

The bandpass over which foreground removal can be performed may affect the errors on the model parameters, even for a fixed total bandpass $B_{\rm tot}$, because the removal of foreground on larger scales allows for more of the strong large-scale (small k) BAO peaks to be included in the fit. However, we find that at the high redshifts that we are considering, increasing $\Delta\nu$ above 8 MHz has little affect on the errors in the recovered values of α. On the other hand, we find that decreasing $\Delta\nu$ increases the systematic uncertainty in the recovered values of α towards the end of reionization. For model fits without the *AP* term, the systematic error exceeds the statistical error when $x_{\rm H\,I} \lesssim 0.2$ (corresponding to redshifts $z \lesssim 6.7$), indicating that our maximum-likelihood indicator is biased. This highlights the potentially significant advantages of including the larger scales accessible with wider bandpasses B.

The systematic component of the errors will in general be sensitive to the functional form chosen to describe the 21 cm PS. We find that the effect of increasing the order of the polynomial used to fit the bias is somewhat degenerate with the chosen value of n_k. For example, with coarser k-space binning of $n_k = 16$ the errors in α decrease by ∼0.5 per cent when the bias is modelled by a fourth-order polynomial rather than a third-order polynomial. This effect is not observed for $n_k = 32$ (see Figs 3 and 4). This implies that sampling of the BAO features must be sufficiently fine. However,

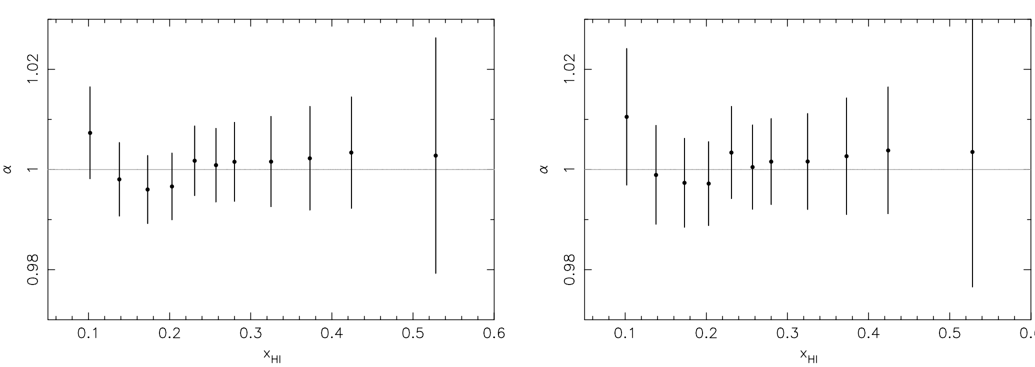

Figure 4. Fitted values and uncertainty for the α using a fit with fourth-order polynomial bias with (left-hand panel) and without (right-hand panel) a quadratic anomalous power term. The error bars represent the 1σ (68.3 per cent) confidence intervals calculated using from the Fisher matrix by marginalizing over all of the other parameters in the fit.

the affect of n_k on the systematic errors in α is only significant for $x_{\rm H\,I} < 0.2$ when the bias is evolving strongly over the range of fitted k values.

5 SUMMARY AND CONCLUSIONS

There has been recent interest in the utility of redshifted 21 cm fluctuations from the IGM as a probe of the mass PS at a range of redshifts (e.g. Bowman et al. 2006; McQuinn et al. 2006; Chang et al. 2008; Mao & Wu 2008; Mao et al. 2008; Wyithe et al. 2008). During the reionization era ($z \gtrsim 6$), the appearance of H II regions generates scale dependence of the bias relating the 21 cm PS to the linear PS. In this paper, we have set out to test the extent to which the scale dependence of the 21 cm bias will interfere with the ability to extract the BAO scale from the PS of 21 cm fluctuations.

We have utilized the results of semi-numerical models for the evolution of the ionized hydrogen distribution on large scales in order to construct an estimate for the 21 cm PS at high redshift. For a model in which the IGM is fully re-ionized by $z = 6$, and assuming the design parameters for a 10-fold expansion of the MWA, we find that the scale-dependent 21 cm bias limits the precision, but not the accuracy, of measurements of the BAO scale in the window $6.5 \lesssim z < 8.0$. We parametrize the bias and anomalous power terms in the 21 cm PS as polynomials, and for the telescope design assumed, find errors on the spherically averaged BAO scale of $\lesssim$1.5 per cent in the window $6.5 \le z \le 7.5$. At redshifts closer to the end of reionization, the strong scale dependence of the 21 cm bias introduces systematic error in the BAO scale, which exceeds the level of the statistical uncertainty for narrower bandpasses ($B < 8$ MHz). We find that the sensitivity of a low-frequency array to the spherically averaged BAO scale decreases with increasing redshift, becoming >2 per cent by $z \sim 8$.

The details of the quantitative results presented in this paper are sensitive to the reionization model assumed. More generally, the constraints available at a particular redshift will be sensitive to the details of the reionization history. The best constraints are likely to be derived from observations of the Universe when the IGM is ~50 per cent ionized – at which time the fluctuations are maximized (Lidz et al. 2008) – but the bias is relatively weakly dependent on scale at the scale of the BAO signal (and hence does not introduce a large systematic error). As a result, if reionization completes earlier than $z \sim 6$, the most precise constraints will be obtained at higher redshift than reported here. However, as the foregrounds become brighter when observing at higher redshift, an early reionization scenario would decrease the maximal precision with which the BAO scale could be measured.

A detailed analysis of the corresponding constraints on the dark energy equation of state is non-trivial and depends on the functional form assumed (Wyithe et al. 2008). We do not explore the translation of the BAO scale to cosmological constraints in this paper. Such an analysis should include independent complementary constraints (e.g. from the CMB), and take account of uncertainties in, for example, the horizon scale (e.g. McQuinn et al. 2006; Mao et al. 2008). Simple estimates of the cosmological constraints from a high-redshift BAO measurement were presented in Wyithe et al. (2008).

In a recent paper Mao et al. (2008) propose a parametrization of the 3d 21 cm PS including peculiar velocity effects which is motivated by the generic form expected for the ionization PS and ionization-matter PS. Our analysis of the accuracy with which the BAO scale may be recovered in the presence of a scale-dependent 21 cm bias is complementary to their detailed discussion of the cosmological constraints available via the redshifted 21 cm PS. Mao et al. (2008) demonstrate that their parametrization can recover the ionization PS constructed from simulations of reionization, and therefore can be used to constrain cosmological parameters from the 21 cm PS. Whilst they mention that their parametrization struggles to describe the high-k ionization PS by a redshift of $z = 7$ when the ionization PS becomes significantly scale-dependent, this is not found to be a problem up to the $k_{\rm max} = 0.2\,{\rm Mpc}^{-1}$ that we consider in this paper. It would be interesting to see how well such a parametrization would perform at the end of reionization in the wavelength range that we have used for our fits.

Our calculations of the constraints on the BAO scale from 21 cm intensity fluctuations are promising when compared to the expected performance of future galaxy surveys. Glazebrook & Blake (2005) show that a dedicated next-generation spectroscopic galaxy survey could measure the BAO scale to an accuracy of ~1 per cent for the transverse component at a redshift $z \sim 3.5$, with a slightly reduced sensitivity to the line-of-sight BAO scale. Limitations in the precision achievable arise due to the large number of galaxies needed to reduce the cosmic variance on the scales at which the BAO signal is expected ($\gtrsim$30 Mpc), combined with the decrease in the number of sufficiently luminous galaxies towards higher redshift. The accuracy with which the BAO scale may be measured via the 21 cm intensity PS is immune to both of these constraints because there is no need to resolve individual objects. Redshifted 21 cm measurements of the PS will instead be limited by cosmic variance owing to the finite size of the field of view and sensitivity to individual modes owing to array configuration and finite collecting area. However, we find that the PS of redshifted 21 cm fluctuations as measured by the MWA5000 could achieve constraints on the BAO scale at $z > 6$ that are comparable to the accuracy which will be available to future galaxy redshift surveys at $z \lesssim 3.5$.

In summary, one potential obstacle in measuring the BAO scale in 21 cm fluctuations during the reionization era is the strongly scale-dependent bias between the 21 cm and mass PS that is produced by the appearance of large ionized regions. In this paper, we have shown that the appearance of ionized regions during the reionization epoch will not inhibit the measurement of the BAO scale during most of the reionization era.

ACKNOWLEDGMENTS

We thank the referee for useful comments. KJR acknowledges the support and hospitality of the Department of Physics, University of Melbourne, and a visiting postgraduate Marie Curie Fellowship hosted by MPA. The research was supported by the Australian Research Council (JSBW). PMG acknowledges the support of an Australian Postgraduate Award.

REFERENCES

Angulo R. E., Baugh C. M., Frenk C. S., Lacey C. G., 2008, MNRAS, 383, 755
Barkana R., Loeb A., 2005a, ApJ, 624, L65
Barkana R., Loeb A., 2005b, ApJ, 626, 1
Blake C., Glazebrook K., 2003, ApJ, 594, 665
Bowman J. D., Morales M. F., Hewitt J. N., 2006, ApJ, 638, 20
Chang T.-C., Pen U.-L., Peterson J. B., McDonald P., 2008, Phys. Rev. Lett., 100, 091303
Cole S. et al., 2005, MNRAS, 362, 505
Corasaniti P.-S., Huterer D., Melchiorri A., 2007, Phys. Rev. D, D75, 062001
Crocce M., Scoccimarro R., 2008, Phys. Rev. D, 77, 023533

Eisenstein D., 2002, in Brown M. J. I., Dey A., eds, ASP Conf. Ser., Vol. 280, Next Generation Wide-Field Multi-Object Spectroscopy. Astron. Soc. Pac., San Francisco, p 35
Eisenstein D. J., Hu W., Tegmark M., 1998, ApJ, 504, L57
Eisenstein D. J. et al., 2005, ApJ, 633, 560
Furlanetto S. R., 2006, MNRAS, 371, 867
Furlanetto S. R., Zaldarriaga M., Hernquist L., 2004, ApJ, 613, 16
Gaztanaga E., Cabre A., Hui L., 2008a, preprint (arXiv:0807.3551)
Gaztanaga E., Miquel R., Sanchez E., 2008b, preprint (arXiv:0808.1921)
Geil P. M., Wyithe J. S. B., 2008, MNRAS, 386, 1683
Giannantonio T., Scranton R., Crittenden R. G., Nichol R. C., Boughn S. P., Myers A. D., Richards G. T., 2008, Phys. Rev. D, 77, 123520
Glazebrook K., Blake C., 2005, ApJ, 631, 1
Hu W., Haiman Z., 2003, Phys. Rev. D, 68, 063004
Kaiser N., 1987, MNRAS, 227, 1
Komatsu E. et al., 2008, ApJS, in press (arXiv:0803.0547)
Lidz A., Zahn O., McQuinn M., Zaldarriaga M., Hernquist L., 2008, ApJ, 680, 962
McDonald P., Eisenstein D. J., 2007, Phys. Rev. D, 76, 063009
McQuinn M., Zahn O., Zaldarriaga M., Hernquist L., Furlanetto S. R., 2006, ApJ, 653, 815
McQuinn M., Lidz A., Zahn O., Dutta S., Hernquist L., Zaldarriaga M., 2007a, MNRAS, 377, 1043
McQuinn M., Lidz A., Zahn O., Dutta S., Hernquist L., Zaldarriaga M., 2007b, MNRAS, 377, 1043
Mao X.-C., Wu X.-P., 2008, ApJ, 673, L107
Mao Y., Tegmark M., McQuinn M., Zaldarriaga M., Zahn O., 2008, Phys. Rev. D, 78, 023529
Mesinger A., Furlanetto S., 2007, ApJ, 669, 663
Okumura T., Matsubara T., Eisenstein D. J., Kayo I., Hikage C., Szalay A. S., Schneider D. P., 2008, ApJ, 676, 889
Page L. et al., 2003, ApJS, 148, 233
Percival W. J., Cole S., Eisenstein D. J., Nichol R. C., Peacock J. A., Pope A. C., Szalay A. S., 2007, MNRAS, 381, 1053
Press W. H., Teukolsky S. A., Vetterling W. T., Flannery B. P., 1992, 2nd edn. Numerical Recipes in C. The Art of Scientific Computing. Cambridge Univ. Press, Cambridge
Seljak U., Zaldarriaga M., 1996, ApJ, 469, 437
Seo H.-J., Eisenstein D. J., 2003, ApJ, 598, 720
Seo H.-J., Eisenstein D. J., 2005, ApJ, 633, 575
Seo H.-J., Eisenstein D. J., 2007, ApJ, 665, 14
Seo H.-J., Siegel E. R., Eisenstein D. J., White M., 2008, ApJ, 686, 135
Shaw J. R., Lewis A., 2008, Phys. Rev. D, 78, 103512
Simpson F., Bridle S., 2006, Phys. Rev. D, 73, 083001
Spergel D. N. et al., 2007, ApJS, 170, 377
Tegmark M., Taylor A. N., Heavens A. F., 1997, ApJ, 480, 22
Trac H., Cen R., 2007, ApJ, 671, 1
Wyithe J. S. B., Loeb A., Geil P. M., 2008, MNRAS, 383, 1195
Wyithe J. S. B., Morales M. F., 2007, MNRAS, 379, 1647
Zahn O., Lidz A., McQuinn M., Dutta S., Hernquist L., Zaldarriaga M., Furlanetto S. R., 2007, ApJ, 654, 12

This paper has been typeset from a TEX/LATEX file prepared by the author.